

TIMING THE NEARBY ISOLATED NEUTRON STAR RX J1856.5–3754

M. H. VAN KERKWIJK¹ AND D. L. KAPLAN²

Accepted for publication in *ApJ (Letters)*, 18 Dec. 2008

ABSTRACT

RX J1856.5–3754 is the X-ray brightest among the nearby isolated neutron stars. Its X-ray spectrum is thermal, and is reproduced remarkably well by a black-body, but its interpretation has remained puzzling. One reason is that the source did not exhibit pulsations, and hence a magnetic field strength—vital input to atmosphere models—could not be estimated. Recently, however, very weak pulsations were discovered. Here, we analyze these in detail, using all available data from the *XMM-Newton* and *Chandra* X-ray observatories. From frequency measurements, we set a 2σ upper limit to the frequency derivative of $|\dot{\nu}| < 1.3 \times 10^{-14} \text{ Hz s}^{-1}$. Trying possible phase-connected timing solutions, we find that one solution is far more likely than the others, and we infer a most probable value of $\dot{\nu} = (-5.98 \pm 0.14) \times 10^{-16} \text{ Hz s}^{-1}$. The inferred magnetic field strength is $1.5 \times 10^{13} \text{ G}$, comparable to what was found for similar neutron stars. From models, the field seems too strong to be consistent with the absence of spectral features for non-condensed atmospheres. It is sufficiently strong, however, that the surface could be condensed, but only if it consists of heavy elements like iron. Our measurements imply a characteristic age of $\sim 4 \text{ Myr}$. This is longer than the cooling and kinematic ages, as was found for similar objects, but at almost a factor ten, the discrepancy is more extreme. A puzzle raised by our measurement is that the implied rotational energy loss rate of $\sim 3 \times 10^{30} \text{ erg s}^{-1}$ is orders of magnitude smaller than what was inferred from the $\text{H}\alpha$ nebula surrounding the source.

Subject headings: stars: individual: (RX J1856.5–3754) — stars: neutron — X-rays: stars

1. INTRODUCTION

The nearby neutron star RX J1856.5–3754 (hereafter J1856) is the closest and brightest of the seven radio-quiet, isolated neutron stars (INS) discovered by *ROSAT* (for reviews, see Haberl 2007 and van Kerkwijk & Kaplan 2007). The INSs have attracted much attention, in part because of the hope that the equation of state in their ultradense interiors could be constrained using their thermal emission. Progress has been slow, however, as adequate fits of the spectra appear to require somewhat contrived models, with the most successful one appealing to hydrogen layers of finely tuned thickness superposed on a condensed surface (e.g., Motch et al. 2003; Ho et al. 2007). A major hindrance is our ignorance of the surface magnetic field: without an observational constraint, models can consider too wide a range to be useful.

We have been able to make some progress, using X-ray observations to determine coherent timing solutions and hence estimates of the dipolar magnetic fields for two of the INS (Kaplan & van Kerkwijk 2005a,b, hereafter KvK05a,b). However, J1856 has resisted such attempts, as its pulsations were so weak that they were discovered only recently, in a long *XMM* observation (Tiengo & Mereghetti 2007, hereafter TM07). TM07 were unable to determine the spin-down rate of the source, finding only a limit of $|\dot{\nu}| < 4 \times 10^{-14} \text{ Hz s}^{-1}$ (at 90% confidence). Here, from a detailed analysis of a larger amount of data, we infer a stronger constraint, and derive a most likely phase-connected solution.

2. OBSERVATIONS

We retrieved all observations of J1856 taken with the *XMM-Newton* (*XMM*) and *Chandra* X-ray Observatories (see Ta-

ble 1), and reprocessed the data from *XMM*'s European Photon Imaging Cameras with PN and MOS detectors using the *epchain* and *emchain* pipelines in SAS version 7.1, and those from *Chandra*'s High Resolution Cameras following standard threads in CIAO version 4.0. For the *XMM* data from 2007 Mar 14, the pipelines gave warnings about odd time jumps in both MOS and PN. We traced these to small sets of duplicated events in the observation data files (ODF), which we removed (our results do not depend on this, or on whether or not we include this observation).

Given that the pulsations are so weak, we tried to optimize the number of source counts. For the PN imaging observations, we decreased the default 150 eV low-energy cutoff to 100 eV, which leads to a 50% increase in source events. For both MOS and PN, we selected source events from a circular region of $37''.5$ radius and with energies below 1 keV (where background flares are negligible). Following normal practice, we included only one and two-pixel events (patterns 0 to 4) with no warning flags for PN, and single to triple events (patterns 0 to 12) with the default flag mask for MOS (removing $< 0.1\%$ of the source counts).

There are also two *XMM* timing observations. For the one with MOS1, we used default settings, and selected single to triple events from columns 315 to 329 with energies less than 1 keV and the default flag mask. The timing observation with PN suffers from frequent bursts of low-energy noise events, and from some high-energy ones due to flares. We identified the former using *epreject*, after which the source dominates the background down to 215 eV for single-pixel events and down to 430 eV for doubles, and up to 600 eV during flares and up to 800 eV otherwise. We selected source events using these criteria from columns 29 to 45.

For the *Chandra* spectra, we extracted not only the zeroth order source events, as done by TM07, but also the about two times more numerous diffracted events. For the former, we used a circle with radius of $3''.6$, while for the latter we

¹ Department of Astronomy and Astrophysics, University of Toronto, 50 St. George Street, Toronto, ON M5S 3H4, Canada; mhvk@astro.utoronto.ca

² Hubble Fellow; MIT Kavli Institute for Astrophysics and Space Research, Massachusetts Institute of Technology, 77 Massachusetts Avenue, 37-664H, Cambridge, MA 02139, USA; dlk@space.mit.edu

TABLE 1
LOG OF OBSERVATIONS AND TIMING MEASUREMENTS

Date	Instr. ^a	ΔT (ks)	N_{ev}	f_b (%)	Z_1^2	a (%)	TOA (MJD)	ν (Hz)
2000 Mar 10....	S	55	36799	1
2001 Oct 8–15...	S	626	320541	2	13	0.9(2)	52193.786169(4)	0.1417396(3)
2002 Apr 8.....	Xm1ti	58	664279	1	34	1.01(17)	52373.011797(2)	0.1417403(17)
2002 Aug 6.....	I	10	9984	9
2002 Sep 3.....	I	55	55632	11
2002 Sep 23....	Ifoc	8	14627
2003 May 4....	I	50	51544	9
2004 Apr 17....	Xpnti	65	377313	9	18	1.0(2)	53113.309266(3)	0.141741(3)
2004 Sep 24....	Xmmf	71	463180	21	1.0(2)	53272.338862(3)	0.1417401(19)	...
2004 Nov 4.....	I	49	47443	14
2005 Mar 23....	Xm1lw	35	378678	17	0.9(2)	53452.558481(3)	0.141738(4)	...
2005 Apr 15....	Xnopn	9	28357
2005 Jun 10....	I	50	65608	2
2005 Sep 24....	X	35	366372	29	1.3(2)	53637.530095(3)	0.141740(3)	...
2005 Nov 13....	I	48	35586	37
2006 Mar 26....	X	70	772404	16	0.65(16)	53821.055080(3)	0.1417375(15)	...
2006 Jun 1.....	I	46	33270	40
2006 Oct 24....	X	73	794684	52	1.14(16)	54032.442099(2)	0.1417412(11)	...
2006 Nov 18....	I	50	31997	40
2007 Mar 14....	Xodf	69	734710	55	1.22(17)	54174.246834(2)	0.1417357(12)	...
2007 Mar 25....	Xmlw	41	488457	31	1.1(2)	54184.467408(3)	0.141739(2)	...
2007 Oct 4.....	X	70	416891	11	0.7(2)	54377.621398(4)	0.1417405(19)	...

NOTE. — Explanation of columns: (date) date of the observation; (ins) instrument code as given in note (a); (ΔT) time between first and last event; (N_{ev}) number of events extracted; (f_b) estimated fraction of events due to background (given only if $\geq 1\%$); (Z_1^2) power of the pulsations; (a) fractional amplitude; (TOA) time of maximum light closest to the mean of all event times; (ν) frequency. Power and timing measurements were derived only for observations with $N_{ev} > 2 \times 10^5$. All uncertainties are 1σ ; those on TOA and ν were derived from fits with a fixed to $0.96(1 - f_b)\%$ (see text).

^a Instrument codes are: (S) *Chandra* High-Resolution Camera for Spectroscopy, used with the Low-Energy Transmission Grating; (I) *Chandra* High-Resolution Camera for Imaging, out of focus; (Ifoc) as (I), but in focus; (X) *XMM* European Photon Imaging Cameras, combining data from the PN and MOS detectors using small-window mode and thin filter; (Xm1ti) as (X), but with MOS1 used in timing mode (for which $f_b = 8\%$); (Xpnti) PN used in timing mode, and both MOS used in full-frame mode and thus ignored; (Xmmf) for MOS, a portion was taken using the medium filters; (Xm1lw) MOS1 used in large-window mode; (Xnopn) only the MOS were used; (Xodf) duplicate frames in the observation data files were removed; (Xmlw) both MOS used in large-window mode.

took rectangles in transmission grating angles (tg_r, tg_d) defined by $|tg_d| < 0^\circ 000531$ (the default for extracting spectra), and $0^\circ 12 < |tg_r| < 0^\circ 42$ (corresponding to $21 \lesssim \lambda \lesssim 73 \text{ \AA}$), where the source clearly dominates the background.

Most of the *Chandra* imaging observations were not taken in focus, and we used ellipses to define regions where the source clearly dominated the background. We extracted events with pulse intensity in the range 1–220 only, since few source events had higher values.

3. INCOHERENT ANALYSIS

Given the fractional amplitude of only $a \simeq 1\%$ of the pulsations in J1856, a $3\text{-}\sigma$ detection requires $\sim 2(3/a)^2 \simeq 2 \times 10^5$ counts (for a single trial at a known frequency). Combining events from the PN and MOS cameras, ten out of eleven *XMM* observations have sufficient counts, while only the long spectrum suffices among the *Chandra* observations. For all of these, we computed Z_1^2 power spectra (Buccheri et al. 1983) for the barycentered event times in a narrow interval around the frequency found by TM07. As can be seen in Fig. 1, the pulsations are detected in all eleven observations. We then fitted the event times for each observation with a sinusoid using Cash (1979) minimization. The resulting fractional amplitudes a , frequencies ν , and inferred arrival times TOA are listed in Table 1.

One sees that the different observations give similar amplitudes. Correcting them for background and statistical bias (the expectation value is $\langle a_m \rangle = ([a_0(1 - f_b)]^2 + 4/N_{ev})^{1/2}$,

where a_m and a_0 are the measured and unbiased amplitudes, N_{ev} the number of counts, and f_b the fraction due to background), and taking a weighted average, the best estimate of the amplitude is $0.96 \pm 0.06\%$ ($\chi^2 = 12.2$ for 10 degrees of freedom [DOF]).

To obtain the best measurements of the phases and frequencies, we refitted each observation holding the amplitude fixed at $a_i = 0.96(1 - f_b)\%$. This yielded the same best-fit values, but uncertainties that were slightly increased for observations for which a_m was high, and decreased for those for which a_m was low. Analytically, this is expected: for small amplitudes, a is not covariant with ν or ϕ , and the uncertainties scale with $(a_m/a_i)^{-1/2}$. In Table 1, we list uncertainties from this second fit.

Fitting the frequencies gives a best-fit frequency derivative $\dot{\nu} = (-5 \pm 4) \times 10^{-15} \text{ Hz s}^{-1}$, with $\chi^2 = 13.7$ for 9 DOF (see Table 2). Clearly, one cannot exclude a constant frequency (which has $\chi^2 = 15.0$ for 10 DOF). The $2\text{-}\sigma$ upper limit is $|\dot{\nu}| < 1.3 \times 10^{-14} \text{ Hz s}^{-1}$ (a factor of three improved over TM07, mostly due to the precise *Chandra* frequency). To verify our result, we also added the Z_1^2 power spectra for a range of frequency derivatives; this led to the same best-fit values, and showed no significant other peaks (see Fig. 1).

4. COHERENT ANALYSIS

Since J1856 has been observed so often, we attempted a coherent analysis, using two different methods. First, we tried finding $(\nu, \dot{\nu})$ combinations that were consistent with both the

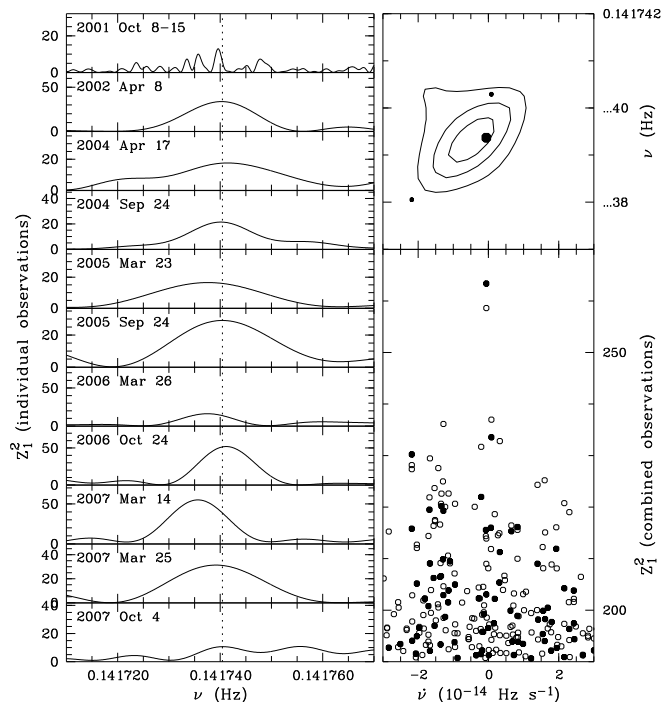


FIG. 1.— Power spectra for RX J1856.5–3754. (*left*) Results for the long individual data sets, near the pulse frequency identified by TM07 (dotted line). The ordinate is scaled such that the mid-point corresponds to a fractional pulsation amplitude $a = (2Z_1^2/N_{\text{ev}})^{1/2} = 1\%$. (*top right*) Incoherently combined power spectra for a range of period derivatives. The contours are at $\Delta Z_1^2 = 2.3, 6.17, 11.8$ (or 1, 2, and 3σ for two parameters of interest). The circles represent the three highest peaks from the coherent analysis. (*bottom right*) Power for coherent combinations of the long observations (open circles) and all observations (filled circles).

frequencies and the arrival times listed in Table 1. For this purpose, we generalised the method of KvK05a to allow us to explore many possible cycle counts between observations (no pair is close enough to give a unique starting solution), and to fit not just arrival times, but also frequencies. In more detail, using the long *Chandra* observation as a reference, we first calculated the number of cycles to the first *XMM* observation for the best-fit frequency and for $\dot{\nu} = 0$. Next, we estimated an uncertainty on the cycle count using a $\pm 5\sigma$ range, with σ determined from the measurement uncertainty on ν and an assumed *a priori* uncertainty of $2 \times 10^{-14} \text{ Hz s}^{-1}$ on $\dot{\nu}$. For each possible cycle count, we calculated a new, much more precise estimate of the frequency, and used it to estimate possible cycle counts for the next observation. We iterated this process, deriving $\dot{\nu}$ as part of the fit for later iterations, until the fit clearly became bad ($\chi^2 > 85$, where including all observations one has 19 DOF: 11 arrival times plus 11 frequencies minus three fit parameters), or until all observations were included. In the end, the best fits did not depend on which observation was used as an initial reference.

The best trial, shown in Fig. 2, resulted in the frequency and frequency derivative listed in Table 2. It has $\chi^2 = 25.7$ for 19 DOF. The fit seems reasonably unique: the two next-best possibilities have $\chi^2 = 49$ and 53, then eight are found between $\chi^2 = 60$ and 70, and thirteen between 70 and 80. Also ignoring frequency information, the best trial is superior: it has $\chi_{\text{TOA}}^2 = 10.7$ for 8 DOF, while the next best has $\chi_{\text{TOA}}^2 = 24$.

As a second method of finding a coherent solution, we calculated $Z_1^2(\nu, \dot{\nu})$ for all data, coherently combining Fourier spectra for individual observations for a range of frequency

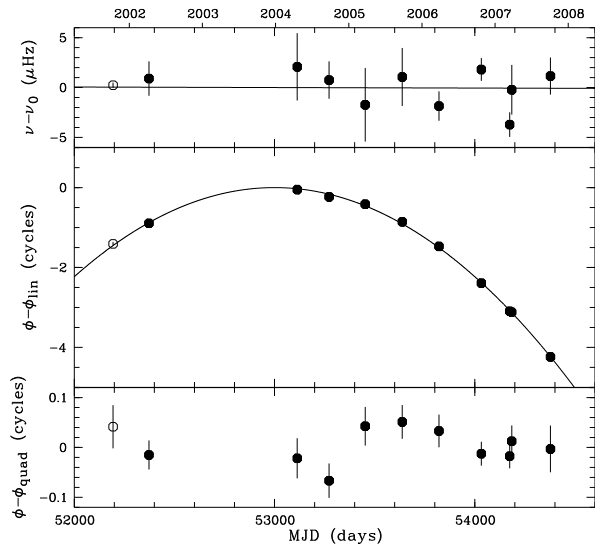


FIG. 2.— Phase and frequency residuals for RX J1856.5–3754. (*top*) Frequency residuals relative to the best-fit quadratic model. (*center*) Phase residuals relative to a linear ($\dot{\nu} = 0$) model. (*bottom*) Phase residuals relative to the best-fit quadratic model. The filled circles represent *XMM* observations, and the open one the long *Chandra* observation.

TABLE 2
TIMING PARAMETERS FOR RX J1856.5–3754

Quantity	Incoherent Value	Coherent Value
Dates (MJD)	52,194–54,377	
t_0 (MJD)	53000.0	53000.000009(3)
ν (Hz)	0.1417393(6)	0.1417393685(5)
$\dot{\nu}$ ($10^{-16} \text{ Hz s}^{-1}$)	-50(80)	-5.98(14)
TOA rms (s)	0.24
χ^2/DOF	13.7/9	25.7/19
P (s)	7.05521(3)	7.05520288(2)
\dot{P} ($10^{-14} \text{ s s}^{-1}$)	20(40)	2.97(7)
\dot{E} ($10^{30} \text{ erg s}^{-1}$)	< 70	3.3
B_{dip} (10^{13} G)	< 7	1.5
τ_{char} (Myr)	> 0.17	3.8

NOTE. — $\tau_{\text{char}} = P/2\dot{P}$ is the characteristic age, assuming an initial spin period $P_0 \ll P$ and a constant magnetic field; $B_{\text{dip}} = 3.2 \times 10^{19} \sqrt{P\dot{P}}$ is the magnetic field inferred assuming spin-down by dipole radiation; $\dot{E} = 10^{45} I_{45} 4\pi^2 \nu \dot{\nu}$ is the spin-down luminosity (with $I = 10^{45} I_{45} \text{ g cm}^2$ the moment of inertia). Uncertainties quoted are twice the formal 1- σ uncertainties. For the incoherent analysis, we used the 2σ lower limit of $|\dot{\nu}| < 1.3 \times 10^{-14} \text{ Hz s}^{-1}$ to derive \dot{E} , B , and τ_{char} .

derivatives (Ransom et al. 2002). This has the advantage that we do not have to decide *a priori* which peaks in the individual power spectra are the correct ones (relevant especially for the long *Chandra* observation; see Fig. 1). For the combined data, the highest peak has $Z_1^2 = 263$ and occurs at the same $(\nu, \dot{\nu})$ found above. This corresponds to a fractional amplitude $a = (2Z_1^2/N_{\text{tot}})^{1/2}/(1 - f_b) = 0.94\%$, consistent with what was found from the individual observations (here, the total number of events $N_{\text{tot}} = 6188356$ and the background fraction $f_b = 1.7\%$). The second and third-highest peaks have $Z_1^2 = 234$ and 230, and correspond to the second and ninth-best solution found using the trial-and-error method, with $\chi^2 = 49$ and 66. The changes in ordering arise because here we included the short observations, which causes the power in the main peak

to increase by $\Delta Z_1^2 = 5$, but that in most other peaks to decrease (see Fig. 1). Folding the shorter observations on the different solutions confirms this conclusion.

In order to verify the uniqueness of our solution, we ran 1000 simulations in which we assumed our best solution and created photon time series corresponding to each of the observations (assuming $a = 0.96(1 - f_b)\%$). We analyzed these in exactly the same way as the real observations. Among the simulations, in 983 out of 1000 cases the correct solution was recovered by the trial-and-error method on the long observations, and in all 1000 using the Z_1^2 power spectra on all data. Inspection of the mis-identification shows that, as expected, it is the addition of the information from the shorter observations that causes the Z_1^2 method to do better.

The best-fit reduced χ^2 slightly exceeds unity, with $\chi^2/\text{DOF} = 1.4$ (the second best solution has $\chi^2/\text{DOF} = 2.6$). This could indicate a fundamental problem, but perhaps more likely reflects that for low-significance detections, outliers in phase and frequency happen more often than expected based on a normal distribution. Indeed, among our 1000 simulations, we find that 211 have best solutions with $\chi^2 > 25.7$, somewhat more than the 140 expected for normal distributions. Alternatively, some unmodeled phase variations may be present, such as seen in other INS (KvK05a,b; van Kerkwijk et al. 2007).

5. RAMIFICATIONS

Assuming the star is spinning down by magnetic dipole radiation, one can use the spin-down rate to infer a magnetic field strength, characteristic age, and spin-down luminosity (see Table 2). We discuss the ramifications below, assuming the coherent solution is the correct one. We compare the results with those obtained for RX J0720.4–3125 and RX J1308.6+2127 (J0720 and J1308 hereafter).

The inferred value of the magnetic field strength of 1.5×10^{13} G is similar to, but somewhat lower than the values of 2.4 and 3.4×10^{13} G found for J0720 and J1308. This lower value might be consistent with the idea that the X-ray absorption features found in the other sources—but not in J1856—are due to proton cyclotron lines or transitions in neutral hydrogen, and that in the lower field of J1856 these are shifted out of the observed band. The inferred value, however, is still somewhat high: calculations by Ho et al. (2007) suggest that for the approximate temperature of J1856 and $B = 1.5 \times 10^{13}$ G (and for a gravitational redshift $z_{\text{GR}} \simeq 0.3$), strong features due to bound-bound transitions should appear at energies of ~ 130 eV (quantum number $m = 0 \rightarrow 1$) and 230 eV ($m = 0 \rightarrow 2$), but none are observed. One could appeal to elements other than hydrogen, but these generally have more bound transitions, thus exacerbating the situation (e.g., Pons et al. 2002; Mori & Ho 2007).

On the other hand, the inferred magnetic field may be consistent with the idea that the surface is condensed, and that

this causes the black-body like spectrum. This depends on the composition: from the recent work by Medin & Lai (2007), it appears that for relatively light elements (based on calculations for carbon and helium), J1856 is far too hot for condensation to be possible. For iron, however, the condensation temperature is relatively high: $kT_{\text{cond}} \simeq 70$ eV for a magnetic field of 1.5×10^{13} G. While we do not know the exact surface temperature of J1856 because of uncertainties in redshift and color correction, the fits of Ho et al. (2007) have $kT_{\infty} \simeq 40$ eV. This corresponds to $kT \simeq 55$ eV at the surface, suggesting that a condensed iron surface is possible. Indeed, this might also be the reason that in early observations, J0720 had a featureless spectrum as well (Paerels et al. 2001). For its field of 2.4×10^{13} G, iron could condense below $kT_{\text{cond}} \simeq 110$ eV, and its observed temperature $kT_{\infty} \simeq 85$ eV corresponds to a surface temperature of ~ 110 eV.

The characteristic age of 4 Myr we derive for J1856 is much larger than the kinematic age of 0.4 Myr inferred assuming an origin in the Upper Scorpius OB association (Walter 2001; van Kerkwijk & Kaplan 2007), and also greatly exceeds simple estimates of the cooling age (~ 0.5 Myr; e.g., Page et al. 2006). Longer characteristic ages—although by a factor of three rather than ten—were also found for J0720 and J1308, which strengthens the suggestion that this is a property common to all isolated neutron stars (KvK05b; see KvK05a for a discussion of possible causes).

Like for J0720 and J1308, the implied spin-down luminosity $\dot{E} \simeq 3 \times 10^{30}$ erg s $^{-1}$ is much smaller than the X-ray luminosity $L_X \simeq 3 \times 10^{32}$ erg s $^{-1}$ (for a distance of 160 pc; van Kerkwijk & Kaplan 2007), consistent with the lack of non-thermal emission. It is also, however, orders of magnitude lower than the independent estimate of $\dot{E} \gtrsim 1 \times 10^{33} (d/160 \text{ pc})^3$ erg s $^{-1}$ made by assuming that the H α nebula associated with J1856 is due to a bow shock, where the pressure from the pulsar wind matches the ram pressure from the interstellar medium (van Kerkwijk & Kulkarni 2001). Indeed, this discrepancy remains even if one considers just the incoherent analysis. The alternate model for the H α nebula considered by van Kerkwijk & Kulkarni (2001)—that it was a moving ionization nebula (Blaes et al. 1995)—was already rejected by Kaplan et al. (2002), because the opening angle of the nebula’s tail did not match observations for distances greater than 100 pc. Thus, our new measurement leaves the nature of the nebula an enigma.

We thank Marc Cropper for convincing us some years ago that, in principle, timing solutions could be derived from sparse data such as ours, and Matthias Ehle and others from the XMM help desk for investigating ODF problems. This work made extensive use of the XMM and Chandra archives, as well as ADS, and was supported by NSERC (MHvK) and NASA (DLK, grant #01207.01-A).

REFERENCES

- Blaes, O., Warren, O., & Madau, P. 1995, *ApJ*, 454, 370
 Buccheri, R. et al. 1983, *A&A*, 128, 245
 Cash, W. 1979, *ApJ*, 228, 939
 Haberl, F. 2007, *Ap&SS*, 308, 181
 Ho, W. C. G., Kaplan, D. L., Chang, P., van Adelsberg, M., & Potekhin, A. Y. 2007, *MNRAS*, 375, 821
 Kaplan, D. L. & van Kerkwijk, M. H. 2005a, *ApJ*, 628, L45 (KvK05a)
 —. 2005b, *ApJ*, 635, L65 (KvK05b)
 Kaplan, D. L., van Kerkwijk, M. H., & Anderson, J. 2002, *ApJ*, 571, 447
 Medin, Z. & Lai, D. 2007, *MNRAS*, submitted, (arXiv:0708.3863)
 Mori, K. & Ho, W. C. G. 2007, *MNRAS*, 377, 905
 Motch, C., Zavlin, V. E., & Haberl, F. 2003, *A&A*, 408, 323
 Paerels, F. et al. 2001, *A&A*, 365, L298
 Page, D., Geppert, U., & Weber, F. 2006, *Nuclear Physics A*, 777, 497
 Pons, J. A. et al. 2002, *ApJ*, 564, 981
 Ransom, S. M., Eikenberry, S. S., & Middleditch, J. 2002, *AJ*, 124, 1788
 Tiengo, A. & Mereghetti, S. 2007, *ApJ*, 657, L101 (TM07)
 van Kerkwijk, M. H. & Kaplan, D. L. 2007, *Ap&SS*, 308, 191

van Kerkwijk, M. H., Kaplan, D. L., Pavlov, G. G., & Mori, K. 2007, ApJ, 659, L149
van Kerkwijk, M. H. & Kulkarni, S. R. 2001, A&A, 380, 221

Walter, F. M. 2001, ApJ, 549, 433